X-ray Crystallographic Structures of Adipocyte Lipid-Binding Protein Complexed with Palmitate and Hexadecanesulfonic Acid. Properties of Cavity Binding Sites[†,‡]

Judith M. LaLonde,[§] David A. Bernlohr,[∥] and Leonard J. Banaszak[*,§]

Department of Biochemistry, School of Medicine, University of Minnesota, Minneapolis, Minnesota 55455, and Department of Biochemistry and the Institute of Human Genetics, College of Biological Sciences, University of Minnesota, St. Paul, Minnesota 55108

Received December 22, 1993; Revised Manuscript Received February 22, 1994[⊕]

ABSTRACT: Adipocyte lipid-binding protein is a 14.6-kDa polypeptide that is responsible for the intracellular trafficking of fatty acids. Its structure previously has been solved in the apo and holo forms complexed with stearate and oleate. To examine the binding of lipids other than those with a carboxylate headgroup, we have determined the structure of ALBP in complex with a sulfonic acid, hexadecanesulfonic acid, and compared its structure with the natural fatty acid analog, palmitate. Crystallographic refinement led to similar models, both with *R*-factors of about 20% and a resolution of 1.6 Å. These results can be compared with earlier studies on C_{18} fatty acids, both saturated and unsaturated. The previously refined complexes with stearate and oleate in combination with the complexes of palmitate and hexadecanesulfonic acid demonstrate specific positions for water molecules bound in the internal cavity. Many of the water-binding sites are present in both the apo form and the holo forms of the protein. With ligand present, a network of 10 internalized water molecules appear to form a hydrophobic hydration region. In spite of the sp^3 geometry of the sulfonic acid derivative, the headgroup occupies the same site as that of the planar carboxylate in natural fatty acids. These results demonstrate that intracellular lipid-binding proteins are capable of binding a wider variety of lipids than previously considered and reveal the importance of interior ordered water molecules in the binding cavity.

Adipocyte lipid-binding protein[1] (ALBP) is a 14.6-kDa polypeptide that resides in adipose cells and is responsible for the intracellular solubilization and trafficking of fatty acids (Matarese & Bernlohr, 1988). ALBP is a member of a larger family known as intracellular lipid-binding proteins or iLBPs[1] (Banaszak *et al.*, 1994). The three-dimensional crystal structures of many members of this family, including murine ALBP (Xu *et al.*, 1993), bovine myelin P2 protein (Cowan *et al.*, 1993), heart muscle fatty acid-binding protein (HFABP) (Zanotti *et al.*, 1992; Müller-Fahrnow *et al.*, 1991), cellular retinol-binding protein II (CRBPII) (Winter *et al.*, 1993), cellular retinol-binding protein (CRBP) (Cowan *et al.*, 1993), rat intestinal fatty acid-binding protein (IFABP) (Scapin *et al.*, 1992), insect fatty acid-binding protein (MFB2) (Benning *et al.*, 1992), and chicken liver fatty acid-binding protein (LFABP) (Scapin *et al.*, 1990), have been determined to varying X-ray resolution.

These three-dimensional structures of the iLBPs include a 10-stranded antiparallel β-sheet arranged in a β-barrel. Within the β-barrel is a cavity formed by the β-strands and two α-helices. The helices are located on the surface covering part of what would be one open end of the barrel. The binding site for hydrophobic ligands is within the cavity, which is closed at the other end by the packing of side chains. Despite the hydrophobic nature of the ligands, the cavity is lined with the side chains of both hydrophobic and polar amino acids. In all of the above structures, the volume of the cavity exceeds that of the ligand by approximately a factor of 2 (Banaszak *et al.*, 1994). Furthermore, because of amino acid sequence variations, the cavity volume varies among the family members. There is little, if any, correlation between cavity volume and the proportion of polar residues in the cavity. The dissociation constants for the hydrophobic ligands also vary from nanomolar to micromolar, again with no discernible relationship between the cavity volume, charge distribution, and binding affinity.

Both with and without ligand, the cavity contains a number of crystallographically ordered water molecules. In the holo forms, the ordered water within the cavity accounts for about 65% of the remaining volume. Comparison of the holo- and apo-IFABP structures (Scapin *et al.*, 1993; Eads *et al.*, 1993) and holo- and apo-ALBP structures (Xu *et al.*, 1993) showed that the presence of ligand is associated with the removal of only a few of the ordered water molecules. Furthermore, the ligand binds with its polar end buried within the cavity.

For ALBP, the crystal structures with bound oleate or stearate (Xu *et al.*, 1993) showed that the carboxylate of the fatty acid is stabilized by salt bridging and hydrogen bonds to R126 and to Y128 and R106 through an intervening water molecule. The scheme therefore appears to involve the burying of a single negative charge (ligand carboxylate) in a cavity near two positive charges (proteins R106 and R126). In addition, titration calorimetry studies of fatty acid-binding to IFABP (Jakoby *et al.*, 1993) and ALBP (J. Trikha, M. Levenson, L. Banaszak, N. Allewell, and D. Bernlohr, manuscript in preparation) suggest that the Gibbs free energy

[†] This work was supported by research grants from the NIH (GM13925) to L.J.B. and the NSF (DMB9118658) to D.A.B.

[‡] Coordinates for HDS–ALBP and PA–ALBP have been deposited in the Brookhaven Protein Data Bank under file names 1LIC and 1LIE, respectively.

* Author to whom correspondence should be addressed.

[§] School of Medicine.

[∥] College of Biological Sciences.

[⊕] Abstract published in *Advance ACS Abstracts,* April 1, 1994.

[1] Adipocyte lipid-binding protein is abbreviated ALBP. It is a member of a larger family of intracellular lipid-binding proteins or iLBP. Other members include bovine myelin P2 protein (P2), human heart muscle fatty acid-binding protein (HFABP), cellular retinol-binding protein (CRBP), cellular retinol-binding protein II (CRBPII), rat intestinal fatty acid-binding protein (IFABP), insect fatty acid-binding protein (MFB2), and chicken liver fatty acid-binding protein (LFABP).

0006-2960/94/0433-4885$04.50/0

associated with binding is largely dominated by enthalpic rather than entropic contributions. The binding enthalpy is presumably derived from Coulombic, hydrogen-bonding, and London-type interactions.

In spite of the fact that crystallographic data is available for multiple members of this family and the fact that several mutant forms have been prepared and analyzed (Stump *et al.*, 1991; Cheng *et al.*, 1991; Jakoby *et al.*, 1993; Sha *et al.*, 1993; Zhang *et al.*, 1992), the correlation between the three-dimensional structure of the cavity, the role(s) of ordered water molecules, and ligand-binding properties remain poorly defined. In an effort to expand our understanding of the structure–function relationship, we have tested the effects of headgroup variation on its positioning in the binding site. The stereochemistry of the binding of a sulfonic acid is compared with that of a normal fatty acid. By comparing all protein atoms and ligand atoms from multiple crystal structures, the effect of headgroup position on overall ligand conformation can be evaluated.

Furthermore, by comparing four different crystal structures, it is possible to evaluate the positioning of bound water molecules in the binding cavity in relation to the conformation of the bound ligand. Internalized water molecules have been observed in all of the hydrophobic ligand-binding proteins (Banaszak *et al.*, 1994; Scapin *et al.*, 1993). The only way to be certain that these bound waters play a significant role in stabilizing the protein and protein:ligand interactions is to demonstrate their appearance in the same locations in the presence of different ligands. That is, they must appear or not appear reproducibly in different crystal structures.

The locations of the internalized water molecules indicate a network that includes the headgroup of the ligand. If the bound water structure is notably altered by variations in the headgroup, then the effect may also be seen in the conformation of the aliphatic chain of the fatty acid. In this study, the structures of ALBP with C_{16} ligands containing different headgroups have been determined. We have crystallized and solved the structures of ALBP with a C_{16} sulfonic acid (hexadecanesulfonic acid) carrying a formal charge of −1 and its natural fatty acid analog, palmitate. By comparing the newly completed structures of the sulfonated and carboxylated C_{16} ligands with the previously reported C_{18} saturated and unsaturated fatty acids (Xu *et al.*, 1993), we are able to study the locations of bound water molecules and the headgroups in the different crystal forms.

MATERIALS AND METHODS

Chemical Methods. Recombinant rat apo-ALBP (Chinander & Bernlohr, 1989) was purified following previously reported methods (Xu *et al.*, 1991). Prior to crystallization, the protein was equilibrated in 12.5 mM Hepes (pH 7.5). ALBP complexes with palmitic acid (PA–ALBP[2]) or hexadecanesulfonic acid (HDS–ALBP[2]) were formed by adding a 1:5 or 1:2 molar excess, respectively. Palmitic acid was obtained from Sigma (no. 5917) as the free acid and added in ethanol to a 10 mg/mL ALBP solution so that the ethanol concentration in the protein solution did not exceed 1 v/v %. Hexadecanesulfonic acid was purchased as the sodium salt from Fluka (no. 52265). HDS was dissolved in 50% (v/v) chloroform in ethanol made acidic with HCl. The HDS solution was added to an empty vial, and the solvent was evaporated. Upon the addition of a 10 mg/mL ALBP solution, the C_{16} sulfonic acid would float to the top of the solution and disappear when mixed. The protein–ligand mixture was gently stirred overnight at room temperature. Crystallization was achieved by adding NaH_2PO_4/K_2HPO_4 buffer (pH 6.6–7.2) to a final concentration of 2.1–3.0 M.

Table 1: Data Collection Statistics

	HDS	PA
no. of crystals	1	1
R_{sym} (I) (%)	2.92	3.63
resolution limit (Å)	1.60	1.6
no. of observations	71512	86794
no. of reflections $I/\sigma_I > 2$	63130	73035
no. of unique reflections	17182	16514
av redundancy	4.2	5.3
av I/σ_I	5.6	3.4
% possible collected to 1.70 Å	99.9	99.9
% possible collected to 1.60 Å	96	96.4

X-ray Methods. X-ray diffraction data was collected to 1.6-Å resolution using a Siemens multiwire area detector with Cu Kα radiation from a Rigaku RU-200 generator equipped with graphite crystal monochromator. Data were collected with a crystal to detector distance of 120 mm and a frame to frame rotation of 0.25°. With the generator operating at 45 kV/200 mA, the counting time per frame was 180 s. Both the PA–ALBP and HDS–ALBP complexes crystallized isomorphously with the previously reported high-resolution apo- and holo-ALBP crystals (Xu *et al.*, 1993). This form of ALBP crystals belongs to the space group $C2$ and occurs with one molecule per asymmetric unit. Unit cell dimensions for PA–ALBP and HDS–ALBP were a = 119.83, b = 37.70, c = 28.48 Å, and β = 92.65° and a = 120.80, b = 37.76, c = 28.60 Å, and β = 92.20°, respectively. Data collection statistics are given in Table 1. Both data sets were very complete and have R_{sym}'s of 3–4%.

Crystal Structure Refinement. For positional or model refinement, the combined X-ray crystallographic and energy minimization was carried out using simulated annealing as implemented in the computer program, X-plor (Brünger *et al.*, 1987). Model building and electron density map inspection used the molecular modeling program, Chain (Sack, 1988). For model adjustment, both $2|F_o| - |F_c|$ and $|F_o| - |F_c|$ electron density maps were calculated and contoured at the 1.0σ and 2.5σ levels, respectively.

The structure of HDS–ALBP was solved using the coordinates of apo-ALBP (Xu *et al.*, 1993), with waters and side chains having alternate conformations removed from the coordinate set used to calculate the initial phases. In addition, the starting temperature factors for all atoms were set to 15.0 Å^2. Calculation of an $|F_o|^1 - |F_o|^2$ difference electron density map clearly showed electron density for the C_{16} sulfonic acid up to C-12. $|F_o|^1$ is the structure factor set derived from the HDS–ALBP crystal, and $|F_o|^2$ represents the X-ray data set from apo-ALBP. Coordinates for the ligand were added to the ALBP coordinates before starting refinement.

The course of refinement is described in Table 2A. The first macrocycle consisted of rigid body refinement and was followed by positional refinement after inspection of the $2|F_o| - |F_c|$ and $|F_o| - |F_c|$ maps and appropriate model adjustments. As can be seen in Table 2A, simulated annealing/refinement proceeded in steps, each step including data shells of increasing resolution. Solvent molecules were added after the resolution was extended to 2.5 Å. Solvent molecules were added on the basis of the following criteria: the spherical appearance of $2|F_o| - |F_c|$ and $|F_o| - |F_c|$, electron density contoured at 1.0σ and 3.0σ levels, and a heteroatom within hydrogen-bonding

[2] Other abbreviations: PA, palmitic acid; HDS, hexadecanesulfonic acid; SA, stearic acid; OA, oleic acid. Complexes with the fatty acid-binding protein ALBP are referred to as PA–ALBP, HDS–ALBP SA–ALBP, and OA–ALBP.

Table 2: Crystallographic Refinement of ALBP/Ligand Structures[a]

cycle	method	resolution (Å)	no. of reflns	av B	no. of atoms	RMSD	R_{free}/R-factor[b]
			A. Refinement of HDS–ALBP				
starting		10–1.6	16785	15.0	1003		0.349/0.346
1	rigid	20–4.0	1115	15.0	1003	0.26	0.260/0.300
2	pos	8–3.5	1541	15.0	1003	0.43	0.291/0.176
3	sa	8–3.5	1541	15.0	999	0.62	0.332/0.156
4	sa	8–3.0	2519	15.0	995	0.59	0.361/0.199
5	sa	8–2.5	4421	15.0	1015	0.57	0.314/0.231
6	sa	10–2.0	8784	13.6	1029	0.46	0.264/0.210
7	sa	10–1.8	11958	14.9	1069	0.21	0.240/0.203
8	pos/bref	10–1.7	14171	16.2	1083	0.16	0.233/0.197
9	pos/bref	10–1.6	16785	16.9	1103	0.07	0.225/0.195
			B. Refinement of PA–ALBP				
starting		10–1.6	15955	17.0	1018		0.354/0.348
1	rigid	20–4.0	1121	17.0	1018	0.13	0.314/0.285
2	pos/bref	10–2.0	8625	14.2	1018	0.21	0.295/0.240
3	sa	10–2.0	8625	12.5	1030	0.31	0.268/0.203
4	sa	10–1.7	13841	14.8	1081	0.40	0.237/0.197
5	pos/bref	10–1.6	15995	16.3	1119	0.41	0.236/0.198
6	pos/bref	10–1.6	15995	15.9	1117	0.35	0.239/0.198

[a] The following abbreviations are used: rigid, rigid body refinement; pos/bref, positional and temperature factor refinement; sa, simulated annealing. [b] R_{free} is defined by Brünger (1993). Ten percent of the F_o's are not used for refinement, but serve as an independent check on improvements in the coordinate set as expressed in the calculated structure factors. R_{free} is the crystallographic R-factor for the reflections omitted from the refinement.

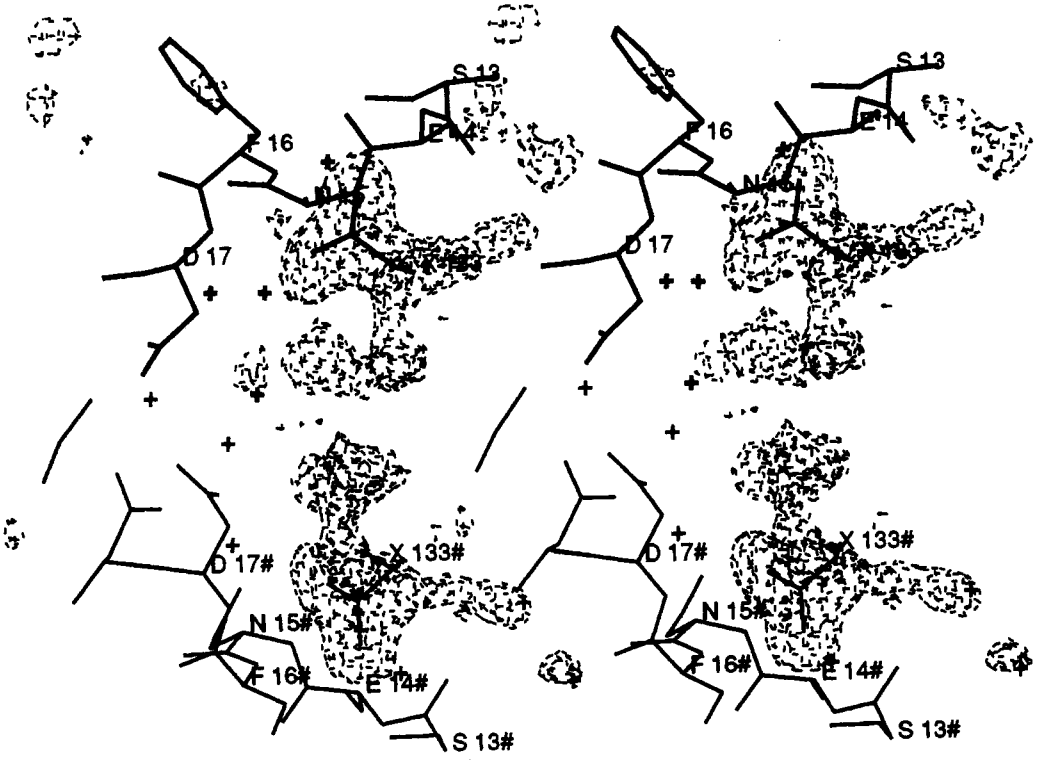

FIGURE 1: Compound X in crystalline ALBP. The stereo diagram illustrates electron density in crystalline ALBP that could not be accounted for by protein or ligand atoms. In the drawing, the unknown compound has been modeled as propionic acid. Since it is located near a crystallographic 2-fold symmetry axis, it appears twice in the illustration. Nearby residues belong to an α-helix and are drawn in bold type. They are labeled by the one-letter amino acid code and the sequence number. The symmetry-related molecule is indicated with thin lines and numbered with a pound sign. The $|F_o| - |F_c|$ electron density map is contoured at the 2.5σ level and was calculated by excluding the coordinates of the unknown compound from the model list.

distance (between 2.7 and 3.2 Å). When the resolution was extended to 1.8 Å, extra electron density suggested that the side chain of C117 was oxidized and it was modeled as SO_2. In the last two cycles of refinement, only alternate rounds of B-factor and positional refinement were performed as the last two shells of data were added. Solvent molecules with B-factors greater than 55 were deleted. Ligand occupancy was refined, whereas solvent occupancy was not. Finally, all solvent molecules were checked in $|F_o| - |F_c|$ omit maps.

For PA–ALBP, the refinement followed a course similar to that of HDS–ALBP, but was limited to six macrocycles. The results are summarized in Table 2B. The initial model was the same as for HDS–ALBP, except that the first 13 carbons of palmitate were included in the coordinate list. The ligand coordinates were derived from a $|F_o|^1 - |F_o|^2$ difference electron density map. Initial B-factors for the starting model were retained from the apo-ALBP model.

For both HDS–ALBP and PA–ALBP with the addition of data below 2.0-Å resolution, a segment of electron density unaccounted for appeared in the $|F_o| - |F_c|$ maps. It appeared above 2.5σ and was located near residues 13–17. This region of electron density shown in Figure 1 has the shape of a carboxylate or a carboxyamide group with some less substantial tails and is located near a crystallographic 2-fold symmetry

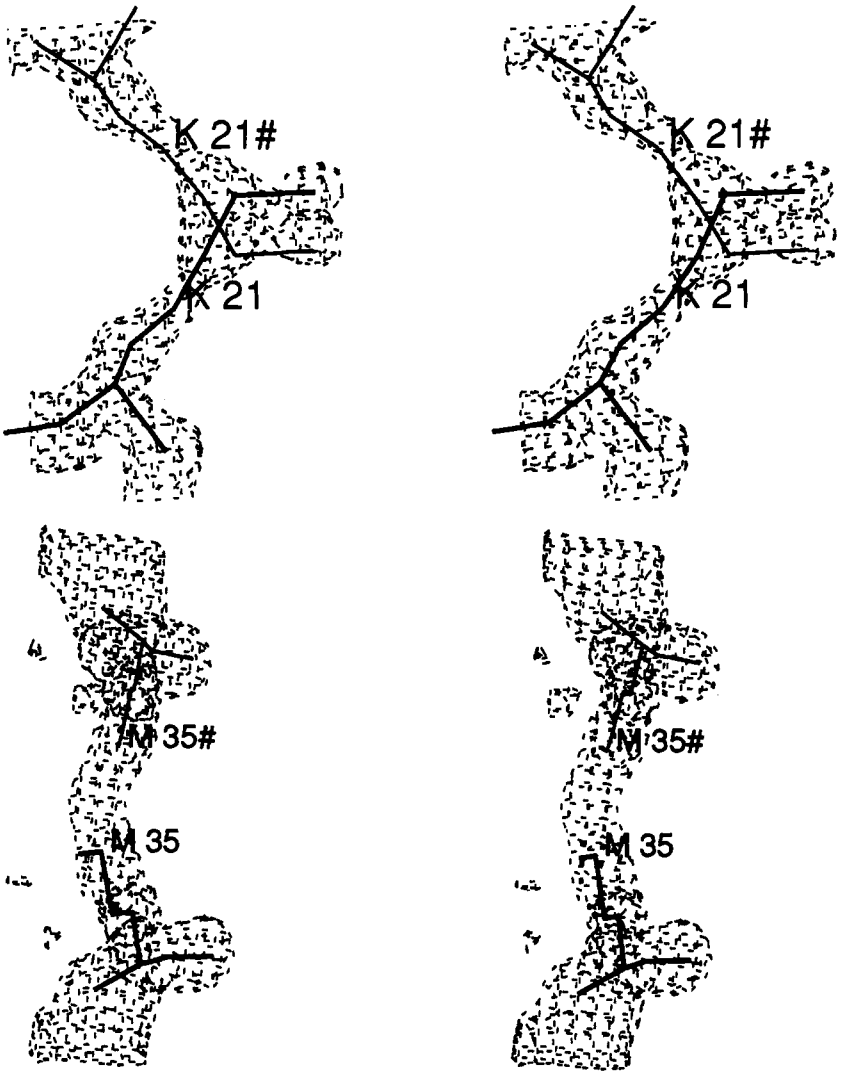

FIGURE 2: Unusual conformations in crystalline forms of ALBP. The stereo diagrams illustrate two questionable molecular sites in crystalline ALBP. They involve residues K21 and M35 and their symmetry mates across the crystallographic 2-fold axis of symmetry. One molecule is represented by bold and the other by thin lines. Electron density maps were calculated using $2|F_o| - |F_c|$ coefficients and were contoured at the 1σ level. (A, top) K21 and its symmetry mate occupy nearly overlapping positions close to the 2-fold axis of symmetry. (B, bottom) M35 is presented as a truncated residue missing the methyl group. The electron density is continuous between the two sulfur atoms, which are separated by 3.16 Å.

axis. The electron density of unknown origin is located within hydrogen-bonding distance from the hydroxyl group of S13 and the main-chain nitrogen of N17. Attempts were made to interpret this density with the nearby side chains of E14 and N15, as well as alternate main-chain tracings. However, all of the alternate models failed to refine properly and returned to the position shown in Figure 1 after simulated annealing.

We have checked earlier crystallographic structures of ALBP with stearate and oleate (Xu *et al.*, 1993). The extraneous electron density was present there as well, but was overlooked during the refinement. The distance extent of the electron density across the 2-fold axis is approximately 11 Å. Only in the crystallographic studies of apo-ALBP is it smaller and less resolved. Since it is essentially contiguous to the 2-fold symmetry axis, by strict interpretation it could be a small molecule that has 2-fold rotational symmetry or one that resides at half-occupancy in two mutually exclusive positions related by symmetry. Moreover, this density has the same shape in both the HDS–ALBP and PA–ALBP structures, eliminating the possibility that it is one of the added ligands.

The constituents of the crystallization buffer, 2.1–3.0 M NaH_2PO_4/K_2HPO_4 and 12.5 mM Hepes, have also been considered as the source. However, the shape of the electron density eliminates derivatives containing a phosphate or a sulfonate group. As shown in Figure 1, the electron density unaccounted for is currently modeled as propionic acid, but the propionic acid model still leaves some unexplained electron density. In total, we estimate that as many as five additional atoms could be included. With this in mind, the mass of the unknown density based on eight hypothetical carbon and two oxygen atoms is approximately 132 Da. For lack of a better explanation, we must assume that it represents a substance that copurifies with ALBP, since it cannot be accounted for by any additives used in purification or crystallization.

During the refinement of both PA–ALBP and HDS–ALBP, two side chains continually presented modeling difficulties, K21 and M35. Both are located near a crystallographic 2-fold axis, and the problems are visible in Figure 2A,B. In earlier crystallographic models of stearate–ALBP and oleate–ALBP (Xu *et al.*, 1993), both K21 and M35 were represented as truncated residues lacking the terminal δ- and ϵ-atoms.

In the present studies, as higher resolution data were added into the refinement, $|F_o| - |F_c|$ electron density appeared at the interface adjacent to the 2-fold axis, suggesting that the side chain and its symmetry-related mate would occupy a common position. Our interpretation for the positions of these side chains in PA–ALBP is shown in Figure 2A,B. A plausible

Table 3: Final Refinement Statistics of Crystalline ALBP Derivatives

	HDS–ALBP	PA–ALBP
A. X-ray Data		
resolution limit (Å)	1.6	1.6
initial R_{free}/R-factor	0.349/0.346	0.354/0.348
final R_{free}/R-factor	0.225/0.195	0.239/0.198
no. of macrocycles	9	6
no. of reflections	16785	15995
no. of atoms	1103	1117
no. of solvent atoms	68	82
av B-factor for protein (Å^2)	15.5	14.3
B. Refined Model Properties		
RMS deviations in geometry		
bonds (Å)	0.021	0.021
angles (deg)	1.473	1.649
dihedrals (deg)	27.958	28.243
impropers (deg)	1.209	1.139

explanation is that alternate conformations exist for K21 and its symmetry-related mate. This interpretation would be consistent with both static and dynamic disorder in the crystal. Thus, the conformations of K21 and its symmetry mate are as shown in Figure 2A with an additional disordered conformation, giving no visible electron density but present with half-occupancy. However, in order to avoid steric interference, this model would require that K21 and its symmetry mate display alternate conformations at any one time. The 2-fold crystallographic symmetry is maintained on a temporal scale.

The $2|F_o| - |F_c|$ density for M35 in PA–ALBP is shown in Figure 2B. Note that the electron density is continuous across the 2-fold axis. As a result, the 2-fold-related sulfur atoms are separated by only 3.16 Å. No reasonable rotamer conformation for M35 could place the terminal methyl group in the electron density. In both PA–ALBP and HDS–ALBP structures, M35 is represented as a truncated residue. Taken as pictured in Figure 2B, the two methionine side chains appear to be close enough to be covalently linked by a single atom through their sulfurs. There is, of course, no chemical evidence for such a structure, so the terminal methyl atom of M35 has been removed from the coordinate list.

The final refinement statistics for both PA–ALBP and HDS–ALBP are given in Table 3. Notice that the R_{free} value (Brünger, 1993) decreased in parallel with the normal crystallographic R-factor. The crystallographic model for PA–ALBP contains 1035 atoms along with 82 solvent molecules. K9, K37, M35, K96, K100, and K120 are included as truncated side chains. HDS–ALBP contains 1035 atoms with 68 solvent molecules, again with side chains for K9, K37, K79, K105, K120, and M35 truncated. In both structures, the side-chain atoms for D47 are represented with two alternating conformations, each present at half-occupancy.

C117 in the maps from both PA–ALBP and HDS–ALBP appears to have additional electron density associated with the side chain. By virtue of the shape and location, we believe that all or a fraction of this side chain occurs in an oxidized form, as SO_2 rather than as SH. The density for the extra two oxygen atoms is comparatively strong. However, close contacts result with the ligands: 3.24 and 3.0 Å in HDS–ALBP and PA–ALBP, respectively. Ion-spray mass spectrometry of a preparation of apo-ALBP in which the C117 was unreactive toward sulfhydryl-directed reagents (Buelt & Bernlohr, 1990) showed an additional mass of 32 Da or two oxygens. The lack of chemical reactivity of C117 toward 5,5-dithiobis(2-nitrobenzoic acid) suggests the oxidation of C117. Although mass spectrometry appears to confirm the presence of additional oxygens, these may be distributed between C1 and C117, as well as the other residues susceptible to oxidation, namely, methionines.

Table 4: Comparisons of the Coordinates of Different Liganded Complexes of ALBP

A. RMS Differences between the Crystalline Coordinates of the ALBPs (Å)

complex	SA–ALBP	OA–ALBP	PA–ALBP	HDS–ALBP
apo-ALBP	0.73	0.75	0.74	0.68
SA–ALBP		0.19	0.51	0.38
OA–ALBP			0.52	0.41
PA–ALBP				0.41

B. RMS Differences between ALBP Ligands (Å)

ligand	OA	PA	HDS
SA	0.23	1.44	1.05
OA		1.40	1.04
PA			0.93

RESULTS

The studies of the two crystal forms of ALBP produced comparable results. For both the C_{16} sulfonic acid and the C_{16} carboxylic acid, demonstrable binding was visible in the electron density maps. Electron density unaccounted for was present in the same place in both crystal derivatives and has been discussed in the previous section. In addition, C117 appears to be partially oxidized, and polymorphic conformations exist for K21 and M35. Moreover, crystallographic refinement led to similar crystallographic models, both with R-factors of about 20% and a resolution of 1.6 Å. Comparisons between the structures of the crystalline protein and the different bound ligands are described below.

A calculation of RMS[3] differences between the apo-ALBP, stearate–ALBP (SA–ALBP), and oleate–ALBP (OA–ALBP) (Xu *et al.*, 1993) and the HDS–ALBP and PA–ALBP structures quantitates the similarity between different liganded states. The comparison data for the structures are presented in Table 4A for all atoms and Table 4B for the bound ligands. A breakdown of the RMS differences for main-chain, side-chain, and solvent atoms (data not shown) indictates that the main-chain positions are virtually identical for the holo and apo forms of ALBP, with RMS differences ranging from 0.12 Å between PA–ALBP and HDS–ALBP to 0.33 Å between OA–ALBP and apo-ALBP. For side-chain positions, the RMS differences vary from 0.79 Å between HDS–ABLP and SA–ALBP to 1.15 Å between SA–ALBP and apo-ALBP. In both cases, RMS differences are somewhat larger between the holo forms of ALBP and apo-ALBP than between the holo forms themselves. RMS differences between solvent positions vary between 0.33 and 0.51 Å.

The somewhat larger RMS difference between side-chain positions can be accounted for by several residues that differ by more than 1 Å. The largest conformational differences in side-chain positions between the HDS–ALBP and PA–ALBP complexes occur at residues K9, V11, K21, R30, L48, F57, K65, I73, and I83. The majority of the observed differences correspond to side-chain rotations on the surface of ALBP. However, most of these variations are within experimental error and may represent different populations of equal energy conformations in the crystalline state. With the exception of F57, none on the above list form contacts with the ligands.

As illustrated in the structures of apo-ALBP and OA–ALBP (Xu *et al.*, 1993), F57 may be a key residue in the binding process. In the apoprotein, it appears to cover a small

[3] The term root-mean-square is abbreviated RMS.

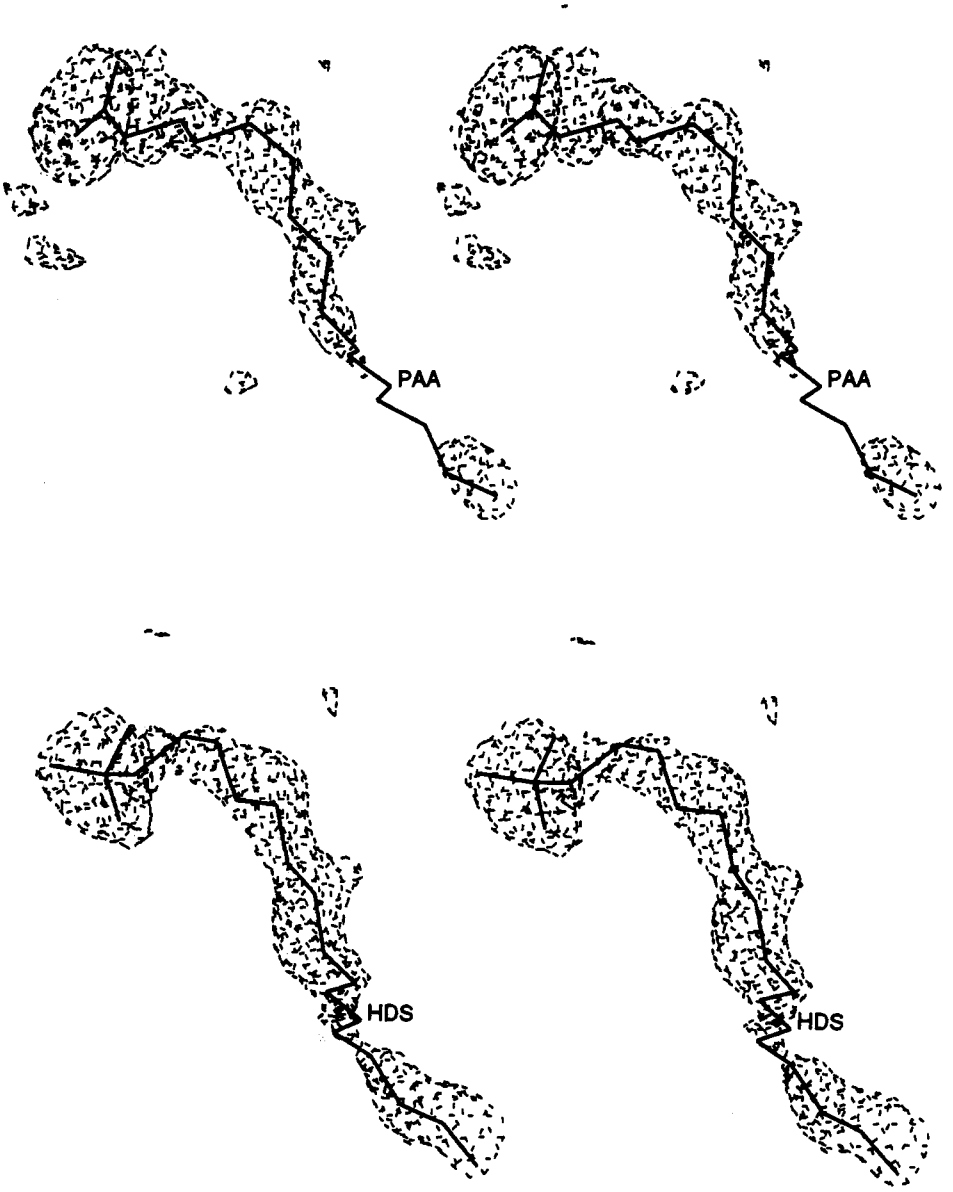

FIGURE 3: Electron density for palmitate and hexadecanesulfonic acid. The electron density shown in both stereo diagrams has a threshold contour level of 1σ, and the maps were calculated using $2|F_o| - |F_c|$ as coefficients. The heavy lines represent the stick model of the bound ligand. (A, top) This diagram shows the results for palmitic acid. (B, bottom) The electron density map and model of hexadecanesulfonic acid are shown.

portal connecting the solvent to the cavity. In contrast, in the holo form it has moved, providing a small opening from the outside to the binding site. In HDS–ALBP, PA–ALBP, and OA–ALBP, the closest contact between F57 and the ligand occurs at the C_β of F57 and not at atoms in its aromatic ring. The contact distance between the C_β of F57 and the respective ligand occurs at 5.11 Å for C_{16} of PA, at 3.84 Å for C_{15} of HDS, and at 3.75 Å for C_{16} of oleate. F57 has high *B*-factors (35–38 Å^2) in all of the crystal structures examined, indicative of the mobility of this side chain.

Differences in Ligand Conformation. The C_{16} studies described here can also be viewed alongside earlier ligand-binding studies using both saturated and unsaturated C_{18} fatty acids (Xu *et al.*, 1993). Analyses and comparisons of the multiple structures define the protein components that are responsible for ligand positioning, the effect of different hydrophilic headgroups, and the bending of the bound hydrocarbon chain. How well the positions of different parts of the ligand are known depends on the electron density maps, which are shown in stereo in Figure 3A,B. Both HDS and PA in crystalline ALBP complexes occupy approximately the same positions in the protein cavity as previously observed with stearic and oleic acids. In addition, both PA and HDS have similar occupancies (0.7 and 0.6) and average *B*-factors (35 and 31 Å^2).

The positioning of atoms belonging to the ligand shows a somewhat larger variation than atoms in the protein itself. The RMS differences between the ligands are given in Table 4B. Note that there is close agreement between the C_{18} ligands, but the positioning appears slightly altered between the C_{16} and C_{18} acids. Despite the differing degrees of saturation, the conformations of stearate and oleate in the SA–ALBP and OA–ALBP structures vary little (RMS difference in distance of 0.2 Å). In addition, stearate displays the kink at C-9 observed in oleate at the location of the cis double bond (Xu *et al.*, 1993). Because the conformations of stearate and oleate are virtually indentical, the comparison of the C_{16} fatty acids with the C_{18} fatty acids is limited to only oleate in this discussion.

Comparison of the positioning of the hydrophobic ligands can also be made visually by studying the stereo diagram shown in Figure 4. The positioning of the ligand in the cavity must be analyzed with certain limitations. The ligand conformations represent a time-averaged position over the

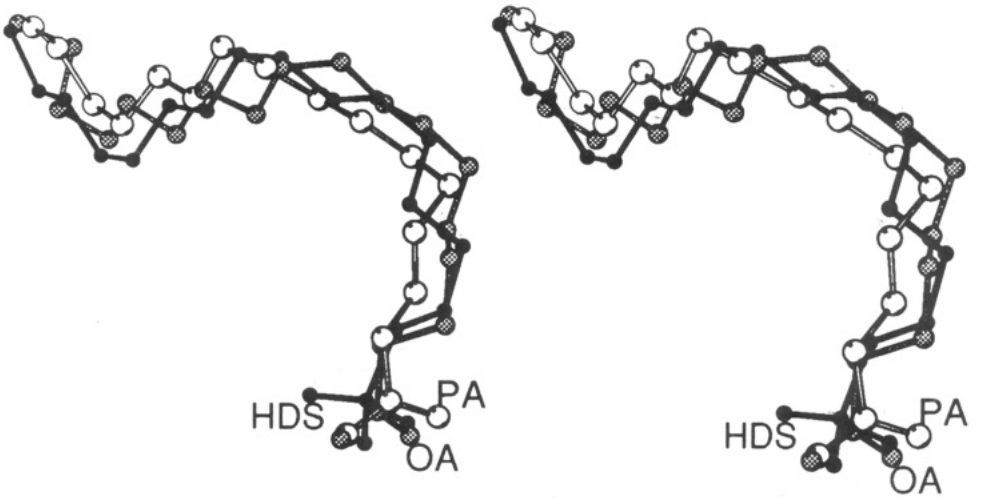

FIGURE 4: Conformation of hydrophobic compounds bound to crystalline ALBP. The stereo diagram contains ball and stick representations of three different compounds bound to crystalline ALBP. The ligands shown are labeled PA for palmitic acid, HDS for hexadecanesulfonic acid, and OA for oleic acid. Crystal data are also available for stearic acid, but the coordinates of the bound ligand were essentially superimposable on those of oleic acid. The models are positioned according to the least-squares superimposition of the protein atoms. The three models are depicted with PA unshaded, HDS in black, and OA indicated as gray ball and stick models.

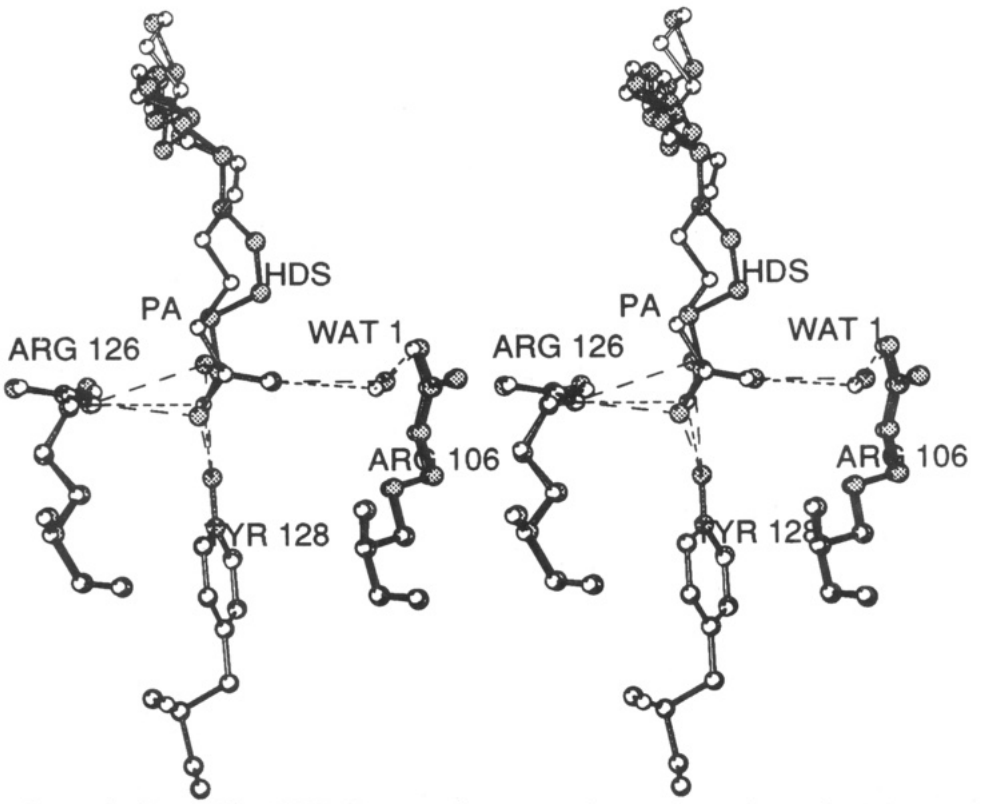

FIGURE 5: Polar headgroup site in crystalline ALBP. The stereo diagram contains superimposed atoms from the crystal structures of both HDS–ALBP and PA–ALBP. The ball and stick models are coded such that PA–ALBP atoms are represented with white spheres, and those belonging to the crystal structure of HDS–ALBP are shaded. The protein atoms that stabilize the polar head group also use the same shading scheme. Hydrogen bonds to PA and HDS are indicated as bold and dashed lines, respectively.

course of the X-ray experiment. Furthermore, it is possible that the fatty acids occupy several subtly similar positions within the electron density that could not be distinguished at the present resolution. Finally, some positional variation is indicated by the *B*-factors, which show an overall increase from head to tail along the aliphatic chains of both PA and HDS. In spite of these uncertainties, fatty acid positioning was quite reproducible from crystal structure to crystal structure. As shown in Figure 4, the time-averaged positions of the ligand indicate that the head to tail distance (14 Å) and the location are identical in all of the crystal structures. Furthermore, each of the ligands displays the same degree of bending (120°) over the length of the aliphatic chain. It follows that the energetic factors contributing to binding are very similar for these compounds.

The binding site can be described in several segments. In examining the polar headgroup, essentially no difference is found in the location of C-1/S-1 for all of the bound ligands. The polar bonding arrangements for both the sulfonic and carboxylate forms are shown in Figure 5. Despite the difference in the hydrogen-bonding geometry of the headgroups for the fatty acid versus the sulfonic acid, sp^2 versus sp^3, respectively, the polar group is accommodated in the same location with no significant changes in side-chain conformation. This is possible by multiple uses of the existing side chains to accommodate the extra oxygen atom.

Table 5: Closest Contacts between Ligands and Amino Acid Side Chains

	PA	HDS	OA
C1			
C2	Cys117	Cys117	Cys117
C3	Cys117	Cys117	Cys117
C4	Cys117	Cys117	Cys117
C5	Wat10	Wat10	Wat3
C6	Wat3	Wat10	Wat10
C7		Asp76	Wat10
C8	Asp76	Asp76	Asp76
C9	Met20	Asp76	Asp76
C10			Lys58
C11	Ala33	Ala75	
C12	Thr29	Ala33	Ala33
C13		Lys58	Ala75
C14	Lys58	Val32	Thr29
C15		Lys58	Lys58
C16	Lys58	Val32	Val32
C17			Lys58
C18			

In PA–ALBP, the carboxylate moiety of palmitate is stabilized at the base of the cavity by forming hydrogen bonds from oxygen 1 to the guanidinium nitrogen of R126 and to the hydroxyl group Y128, while oxygen 2 hydrogen bonds to an amino nitrogen of R106 through an intermediary water molecule. Interestingly, in the case of HDS, the extra oxygen is accommodated by pairs of bifurcated hydrogen bonds. As is visible in Figure 5, both oxygen atoms 1 and 2 form two hydrogen bonds each: the first to R126 and the second to Y128 for a total of four hydrogen bonds. One of the oxygens in HDS behaves identical to that in a carboxylate headgroup and forms an analogous hydrogen bond with R106 via a water molecule.

Since the aliphatic chain of the bound ligand is always bent, it is of interest to analyze the chain dihedral (torsional) angles in more detail. In complexes of ALBP with both PA and HDS, there are the same number of synclinal (−60, +60) and anticlinal (−120, +120) dihedral angles, four and one, respectively. The number of antiplanar (+180, −180) dihedral angles in PA is nine and in HDS is ten. Because the numbers of synclinal, anticlinal, and antiplanar dihedral angles are approximately the same, the potential energies of the conformations of both PA and HDS would be similar. As noted earlier, PA, HDS, and OA span an equal distance from head to tail in the binding cavity, approximately 14 Å. The head to tail length of the fatty acid has an inverse relationship to the number of anticlinal dihedral angles. In the cases of PA and HDS, the number of observed anticlinal dihedral angles is consistent with the common head to tail span between the different ligands.

Examination of fatty acid–protein interactions indicates that the ligands contact a common set of amino acid side chains in the cavity. The closest amino acid contacts, at a distance of 4.0 Å or less, between each carbon atom along the aliphatic chains of PA, HDS, and OA are included in Table 5. The most conserved contacts occur at C-2, C-3, and C-4 with C117 and at C-8 with D76. These are van der Waals contacts between an oxygen of the oxidized C117 and a carboxylate oxygen from D76.

In order to analyze all of the interactions in the different crystal structures, we have divided them into two sets. The first group is defined by the fact that these residues are found to form contacts with all of the ligands tested. Residues in this category include M20, V32, A33, M40, K58, A75, D76 C117, R126, and Y128. They provide atoms in the primary ligand-binding framework. The second category contains those amino acids that make contacts to only some of the ligands. These are atoms in the side chains of F16, T29, F57, R78, I104, and V115. In order to simplify the description of the location of these amino acids, the cavity can be viewed as a sphere. Viewed parallel to the aliphatic chain from its head to its tail, the sphere can be divided vertically into two hemispheres, each corresponding to a right and left face of the fatty acid. The residues of the primary and secondary frameworks are located predominantly in the left hemisphere relative to the ligand. Only residues K58, D76, I104, and R78 make contacts in the upper quadrant of the right hemisphere.

Analysis of the total number of polar and nonpolar van der Waals contacts between the aliphatic chain of the ligand and protein atoms gives unexpected results. The number of polar and nonpolar contacts for PA, HDS, and OA are as follows: 13 and 17; 10 and 18; and 16 and 10, respectively. The reversal in the ratio of polar to nonpolar contacts in the case of OA is associated with a lower number in the nonpolar category made from C-8 to C-12 in comparison to the numbers observed in PA and HDS in this region. The double bond in OA is located between C-9 and C-10. Carbons 8–12 in PA and HDS make more extensive contacts with the hydrophobic atoms of A75 and D76 than is observed with OA. The larger number of polar neighbors, however, observed with OA can only be accounted for by contacts with additional nonconserved water molecules observed in the OA structure near C-13, C-15, and C-17.

Solvent Structure. With the different geometry between sulfonate (sp^3) and carboxylate (sp^2), the possibility exists for changes in the water network common to all liganded forms of ALBP. A total of 68 and 82 water molecules was located in the HDS–ALBP and PA–ALBP structures, respectively. The waters were refined at full occupancy and have average *B*-factors of 31 and 33 Å^2 in the crystal structures of PA–ALBP and HDS–ALBP, respectively. A comparison of the waters in these two structures, as well as those in the SA–ALBP and OA–ALBP structures, identified a total of 59 conserved water molecules. This represents 86%, 72%, 61%, and 64% conserved water positions in the HDS–, PA–, SA–, and OA–ALBP structures, respectively.

The nonconserved or variable water sites in the individual structures are not clustered in any one region of the molecule. Some of the nonconserved waters are located near lysine residues that exhibit differing conformations in the various crystal structures. In these cases, the different solvent positions reflect only the alteration in the local environment. Of the 59 conserved water molecules in the crystalline state, 10 reside in the protein cavity. The remainder are located on the surface of the protein and form typical hydrogen-bonding contacts with polar residues.

To provide easy recognition of the solvent positions and protein side chains, a simple nomenclature system has been adopted. Water molecules were numbered according to the residues with which they form their closest contact. For example, water 1095 represents the first water in hydrogen-bonding contact with residue 95. Water 2095 represents the second water molecule bound to residue 95. Waters composing the secondary shell of hydration are numbered similarly according to the closest water molecules to which they are bound. Therefore, a water bound to water 1071 and not to any nearby amino acid residues would be numbered 9071; numbers 7000–9000 indicate the secondary shell of hydration. This numbering system can be found in the coordinate files of HDS–ALBP and PA–ALBP submitted to the Brookhaven Protein Data Bank. The 10 conserved waters within the cavity are shown in Figures 6 and 7, where they are numbered 1–10 to simplify discussion.

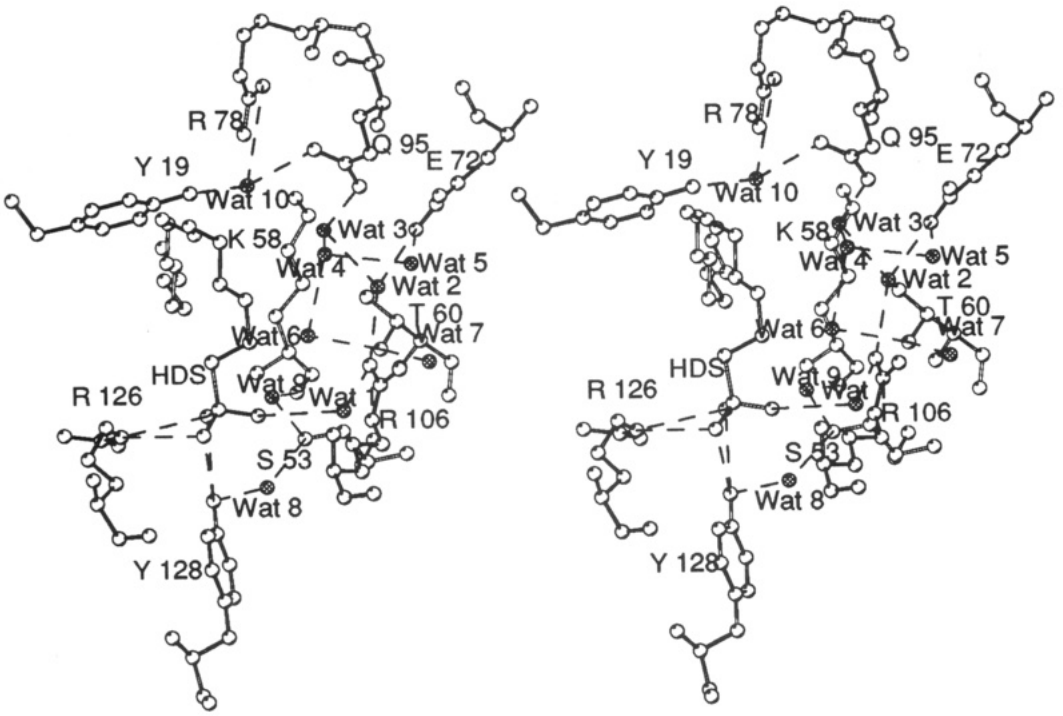

FIGURE 6: Stereo diagram of the solvent molecules conserved in the ligand-binding cavity of ALBP. The solvent molecules, bound fatty acid, and appropriate side chains present in the cavity are shown in stereo. The conserved water molecules are identified by the labels Wat1 through Wat10. Water molecules are shaded gray, while amino acid residues are white. The numbering for Wat1–Wat10 on the coordinate file is as follows: Wat1, 1106; Wat2, 2072; Wat3, 2095; Wat4, 1075; Wat5, 1072; Wat6, 2060; Wat7, 1060; Wat8, 1128; Wat9, 1053; Wat10, 1095.

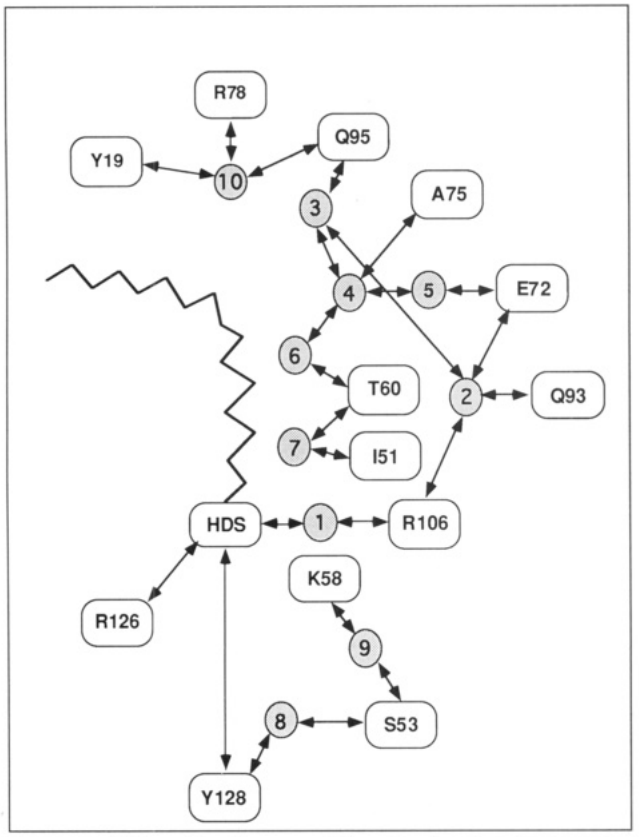

FIGURE 7: Schematic diagram of the solvent molecules conserved in the ligand-binding cavity of ALBP. The hydrogen-bonding network between the 10 conserved water molecules within the cavity of ALBP is shown schematically. The waters are shaded gray and numbered 1–10. The headgroup of the C_{16} sulfonic acid is indicated by HDS. Other amino acid side chains of ALBP are denoted by the one-letter code and their amino acid sequence number.

The positions of the conserved water molecules in the cavity are shown in Figures 6 and 7. These 10 conserved sites are also observed in crystalline apo-ALBP. However, in the apo form, water 1 is shifted away from R106 toward a methionine side chain, M40. These crystallographic results show that ligand binding is not directly responsible for the network of water molecules. Rather, the water positions in the cavity that are in contact with ligand are the product of networks introduced by intervening polar side chains. They are part of the folded protein in both the apo and holo forms.

As shown in stereo in Figure 6 and schematically in Figure 7, the network is numbered beginning with water 1 (1106), which forms a bridging hydrogen bond from oxygen 2 of the ligand to R106. This is present in both carboxylated and sulfonated ligands. The network continues in two segments. It involves the polar interactions with the headgroup and a series of water molecules linked to polar side chains. Overall, the interconnecting waters encompass a major part of the ligand-binding site.

Although not clearly visible in Figures 6 and 7, some of the water sites are in contact with parts of the hydrocarbon chain. Waters 3 (2095), 4 (1075), and 10 (1095) form a complementary surface with the fatty acid near C-5 and C-6. The distances between these waters and the aliphatic chain are listed in Table 6. Water 3 (2095) contacts C-5 and C-6 in both PA and OA, while only contacting C-5 in HDS. Water 10 (1095), however, forms contacts with both C-5 and C-6 in PA and HDS, while contacting C-6 and C-7 in crystalline OA–ALBP. Water 4 (1075) contacts C-6 in PA, but does not make similar contacts with HDS or OA. The differences in chain length and dihedral angles account for this difference in water contacts with the aliphatic chain. This set of polar van der Waals contacts between water molecules and the aliphatic chain of the ligand has also been observed in two other proteins belonging to this family (Scapin *et al.*, 1993).

Water 10 (1095) forms the closest van der Waals (3.0–3.2 Å) contact with C-5 in PA and HDS and with C-6 in OA and is connected to the network via a hydrogen bond to E95. Water 10 (1095) makes two other hydrogen bonds: one to the hydroxyl of Y19 and the second to the amino group of R78. Interestingly, Y19 is the site of phosphorylation by the

Table 6: Contact Distances between Ligands and Conserved Water Molecules

PA atom	water	distance (Å)	HDS atom	water	distance (Å)	OA atom	water	distance (Å)
PAA C5	Wat3	3.39	HDS C5	Wat3	3.76	OA C5	Wat3	3.69
PAA C6	Wat3	3.37				OA C6	Wat3	3.31
PAA C5	Wat10	3.23	HDS C5	Wat10	3.08	OA C6	Wat10	3.02
PAA C6	Wat10	3.85	HDS C6	Wat10	3.88	OA C7	Wat10	3.25
PAA C6	Wat4	3.66						

activated kinase domain of the insulin receptor (Bernier *et al.*, 1987; Hresko *et al.*, 1988; Buelt *et al.*, 1991). Therefore, water 10 (1095) may stabilize the protein conformation in the unphosphorylated form, with R78 as a likely candidate to interact with the charged phosphate moiety in the phosphorylated form.

Key side chains involved in maintaining the water network are T60, E72, and Q95. All form hydrogen bonds to at least two different water molecules, stabilizing six of the ten conserved water molecules. These three residues are highly conserved polar sites in the hydrophobic ligand-binding protein family (Banaszak *et al.*, 1993). In terms of the spherical cavity as described above, all 10 of the conserved waters are located in the right hemisphere relative to the ligand. The 16 residues that form contacts with the fatty acid, as described above, are mainly located in the left hemisphere. In the right hemisphere, contacts between amino acid side chains and the fatty acid occur only in the upper quadrant, while waters form contacts solely in the lower quadrant.

There is one other interesting aspect of the conserved water network. The 10 conserved solvent molecules are connected to the surface of the protein through a hydrogen bond from water 5 (1072) to a water located in the gap between β-strands D and E. These two β-strands have an abnormally large gap between them (6.7 Å) and therefore have no interstrand hydrogen bonds. Instead, four water molecules bridge the two strands. These gap water molecules are then linked to the cavity system described above. Thus, conserved waters 2 (2072), 3 (2095), 4 (1075), 5 (1072), 6 (2060), and 7 (1060) form a shell of hydration between the surface of the protein and the aliphatic face of the ligand.

DISCUSSION

In the case of the hydrophobic ligand-binding proteins, some of the binding selectivity resides in the interactions ALBP makes with the ligand headgroup. However, for ALBP and this entire family of proteins, most of the ligand is simply an aliphatic chain. Structural factors contributing to the binding stabilization are less obvious than those for polar clusters of atoms normally associated with the more common water-soluble biochemicals. In order to better understand elements of the structure contributing to binding, and to design new binding capacities to these proteins, we have analyzed a number of crystal forms of ALBP with different bound ligands. By comparing the results of multiple crystallographic studies, we have been able to obtain insights into the binding process. This is particularly true for solvent molecules where multiple structures provide a degree of reliability missing in a single-crystal study. When the same water sites are found in multiple crystal structures, the nature of these locations becomes less tenuous.

Analysis of the solvent positions in the cavity reveals that a set of conserved water-binding sites is maintained regardless of the presence or absence of ligand and the nature of the headgroup. Ten reproducible water sites are present. This has implications for two properties: the native protein conformation and the nature of the ligand-binding site. The water molecules are present in the cavity because of the presence of internalized polar residues. We believe that internalized polar residues are important for the maintenance of the three-dimensional structure. In simple terms, if these internal polar residues were to be substituted with hydrophobic residues, hydrophobic forces would dominate during protein folding. Therefore, the protein would have a nonpolar core that would tend to collapse into a hydrophobic center typical of most globular proteins, eliminating the cavity.

With regard to ligand binding, the internalized water network appears to interact directly with hydrophobic compounds and forms a complementary surface to segments of the ligand. This network is essentially invariant; the average RMS difference between the four sets of conserved water molecules is 0.26 Å. Furthermore, no change in water structure occurs when the carboxylic moiety is exchanged for a sulfonic acid group. Secondly, despite differences in the length of the fatty acid, the water–fatty acid contacts generally are maintained. Thus, the water molecules serve as fixed extensions of the amino acid side chains rather than as an adjustable surface that accommodates various ligand-binding modes.

The polar residues within the cavity that stabilize the hydrogen-bonded water network, Y19, T60, E72, R78, and Q95, are highly conserved in a subfamily of the iLBPs consisting of ALBP, P2, HFABP, Mal-1, MDGI, and shark FABP (Banaszak *et al.*, 1994). This sequence homology strengthens the hypothesis mentioned above that the arrangement of internally bound water molecules is a consequence of the stabilization of internal polar and charged side chains associated with protein folding. However, several of the conserved water molecules anchored by these polar residues form van der Waals contacts with the aliphatic chain of the ligand. van der Waals contacts between CH_x groups and water molecules have been observed in neutron diffraction studies (Savage, 1986).

Comparison of the two geometries of the bound sulfonic acid versus the carboxylate shows that an extra oxygen or hydrogen-bond acceptor in HDS can easily be accommodated within the cavity of ALBP. The carboxylate headgroup normally interacts with two arginines and one tyrosine side chain. The side-chain conformations of the arginine residues do not change with sp^3 versus sp^2 headgroups. Furthermore, no change in the distribution of the water molecules within the cavity accompanies the binding of the sulfonic acid. Instead, HDS positions itself in the same location as the carboxylated fatty acids, with only a minor adjustment of the S-1 position of HDS relative to the C-1 position of PA.

In a sense, the three oxygens of HDS form the same set of contacts as with a carboxylate, but in the case of the sulfonated headgroup, bifurcated hydrogen bonds are used to accommodate the difference in the number of oxygen atoms. Visible in Figures 6 and 7 is the interaction of the carboxylated fatty acids with R106 through hydrogen bonds with an intervening water molecule. One might have predicted that the sulfonic acid would interact directly with the two charged arginine residues, 106 and 126. The fact that this change is not observed supports the view that the distribution of hydrogen-bond acceptor and donor positions is fixed within the cavity and

that ligands with altered polar headgroups can only be accommodated if the ligand headgroup accepts the hydrogen-bonding "rules".

The bent conformations of the C_{16} and C_{18} fatty acids as bound to ALBP have been compared. Because of the resolution of the X-ray studies, it is difficult to pinpoint locations in the hydrocarbon chain that cause the clearly observed bending. The conformers of a hydrocarbon chain differ little in energy, and bending can only be caused by dihedrals differing from all-trans (antiplanar). We have asked the question whether it is single or multiple torsional angles that are responsible for the bend. The answer is not straightforward, but it appears that the change in direction cannot be attributed to the C-9/C-10 bond angle (Δ in oleate). The curvature appears to begin earlier at C-5/C-6.

We have tried to determine the underlying cause of the bending. Is it due to protein atoms, the water network, or both? The contacts at C-5/C-6 in the crystal structures with palmitic, hexadecanesulfonic, and oleic acids are with waters 10 (1095) and 3 (2095). Hence, it is possible that these waters are critical in forming the surface that results in the bend. What seems irrefutable from the X-ray studies is the fact that both the C_{16} and C_{18} ligands maintain the same head to tail distance of 14 Å. In addition, the C_{18} fatty acids have virtually the same conformation regardless of the degree of saturation (Xu *et al.*, 1993). The $C_{18:0}$ fatty acid (i.e., stearate), adopts a synplanar dihedral angle between C-9 and C-10, as observed in $C_{18:1}$ (i.e., oleate) (Xu *et al.*, 1992). The adoption of this dihedral angle foreshortens the length of the fatty acid. The C_{16} fatty acids in this study, however, do not display this same synplanar dihedral angle. In light of this observation, it appears that, in the case of the saturated C_{18} fatty acid, the loss of energy associated with adopting a synplanar dihedral angle is preferable to allowing the aliphatic chain to protrude too much at the surface of the protein.

In summary, a framework of conserved contacts between the ligand and ALBP amino acids has been identified in multiple crystal structures. This framework includes both hydrophilic and hydrophobic residues and water molecules, with the numbers of polar and nonpolar contacts being approximately equivalent. The water molecules, which in general are the most difficult to characterize, appeared at the same locations in four different crystal structures. The waters are networked and actually form part of the ligand-binding cavity. The X-ray crystallographic studies also confirm the hydrocarbon curvature that has been observed in ALBP and other family members (Xu *et al.*, 1993; Banaszak *et al.*, 1994). Finally, the crystallographic results reported here establish that sulfonated compounds will bind to a site previously considered to associate only with carboxylates and suggest that ligands other than simple fatty acids may be physiological ligands for this class of proteins.

ACKNOWLEDGMENT

We are grateful to associates in the Banaszak and Bernlohr laboratories, especially C. Kane, for their helpful discussions. The authors thank Per Kraulis for the use of the drawing program MOLSCRIPT. We are grateful to Ed Hoeffner for his continued help in the use of the computing and X-ray diffraction instrumentation. We are indebted to the Minnesota Supercomputer Institute for the use of their resources, which were utilized during the refinement.

REFERENCES

Banaszak, L., Winter, N., Xu, Z, Bernlohr, D. A., Cowan, S., & Jones, T. A. (1994) *Advances in Protein Chemistry* (Schumaker, V., Ed.) Vol. 45, pp 89–149, Academic Press, San Diego, CA.

Benning, M. M., Smith, A. F., Wells, M. A., & Holden, H. M. (1992) *J. Mol. Biol. 228*, 208–219.

Bernier, M., Laird, D. M., & Lane, M. D. (1987) *Proc. Natl. Acad. Sci. U.S.A. 84*, 1844–1848.

Buelt, M. K., & Bernlohr, D. A. (1990) *Biochemistry 29*, 7408–7413.

Buelt, M. K., Shekels, L. L., Jarvis, B. W., & Bernlohr, D. A. (1991) *J. Biol. Chem. 266*, 12266–12271.

Brünger, A. (1993) *Acta Crystallogr. D49*, 24–46.

Brünger, A. T., Kuriyan, J., & Karplus, M. (1987) *Science, 235*, 458–460.

Cheng, L., Qian, S., Rothschild, C., Avignon, A., Lefkowith, J., Gordon, J., & Li, E. (1989) *J. Biol. Chem. 266*, 24404–24421.

Chinander, L. L., & Bernlohr, D. A. (1989) *J. Biol. Chem. 264*, 19564–19572.

Cowan, S. W., Newcomer, M. E., & Jones, T. A. (1993) *J. Mol. Biol. 230*, 1225–1246.

Eads, J., Sacchettini, J., Kromminga, A., & Gordon, J. (1993) *J. Biol. Chem. 268*, 26375–26385.

Hresko, R. C., Bernier, M., Hoffman, F. D., Flores-Riveros, J., Liao, K., Laird, D. M., & Lane, M. D. (1988) *Proc. Natl. Acad. Sci. U.S.A. 85*, 8835–8839.

Jakoby, M. G., Miller, K. R., Tonner, J. J., Bauman, A., Cheng, L., Lie, E., & Cistola, D. P. (1993) *Biochemistry 32*, 872–878.

Matarese, V., & Bernlohr, D. A. (1988) *J. Biol. Chem. 263*, 14544–14551.

Müller-Fahrnow, A., Egner, U., Jones, T. A., Rüdel, H., Spener, F., & Saenger, W. (1991) *Eur. J. Biochem. 199*, 271–276.

Sack, J. (1988) *J. Mol. Graph. 6*, 224–225.

Savage, H. (1986) *Biophys. J. 50*, 967–980.

Scapin, G., Spadon, P., Mammi, M., Zanotti, G., & Monaco, G. (1990) *Mol. Cell. Biochem. 98*, 95–99.

Scapin, G., Gordon, J. I., & Sacchettini, J. C. (1992) *J. Biol. Chem. 267*, 4253–4269.

Scapin, G., Young, A. C. M., Kromminga, A., Veerkamp, J. H., Gordon, J. I., & Sacchettini, J. C. (1993) *Mol. Cell. Biochem. 123*, 3–13.

Sha, R., Kane, C. D., Xu, Z., Banaszak, L., & Bernlohr, D. (1993) *J. Biol. Chem. 268*, 7885–7892.

Stump, D. G., Lloyd, R. S., & Chytil, F. (1991) *J. Biol. Chem. 266*, 4622–4630.

Winter, N., Bratt, J., & Banaszak, L. (1993) *J. Mol. Biol. 230*, 1247–1259.

Xu, Z., Buelt, M., Banaszak, L., & Bernlohr, D. (1991) *J. Biol. Chem. 266*, 14367–14370.

Xu, Z., Bernlohr, D., & Banaszak, L. J. (1992) *Biochemistry 31*, 3484–3492.

Xu, Z., Bernlohr, D., & Banaszak, L. J. (1993) *J. Biol. Chem. 268*, 7874–7884.

Zanotti, G., Scapin, G., Spadon, P., Veerkamp, J. H., & Sacchettini, J. C. (1992) *J. Biol. Chem. 267*, 18541–18550.

Zhang, J., Liu, Z.-P., Jones, T., Gierasch, L., & Sambrook, J. (1992) *Proteins: Struct. Funct. Genet. 13*, 87–99.